



Quantitative breast lesion classification based on multichannel distributions in shear-wave imaging

Chung-Ming Lo ^{a, b}, Yi-Chen Lai ^{c, d}, Yi-Hong Chou ^{c, d} , Ruey-Feng Chang ^{b, e}

Show more

<https://doi.org/10.1016/j.cmpb.2015.09.004>

[Get rights and content](#)

Highlights

- A **computer-aided diagnosis** (CAD) system based on the quantified color distributions in **shear wave elastography** (SWE) was developed.
- The combination of the proposed CAD system using SWE features and **BI-RADS** assessment would provide a promising diagnostic suggestion.
- **Spatial correlation** was combined with the kPa-weighted color information as a feature to reduce the influence of noises far from tumor.

Abstract

Background and objectives

A computer-aided diagnosis (CAD) system based on the quantified color distributions in shear-wave elastography (SWE) was developed to evaluate the malignancies of breast tumors.

Methods

For 57 benign and 31 malignant tumors, 18 SWE features were extracted from regions of interest (ROI), including the tumor and peritumoral areas. In the ROI, a histogram in each color channel was described using moments such as the mean, variance, skewness, and kurtosis. Moreover, three



Results

The performance of the CAD system achieved an accuracy of 81%. Combining the CAD system with a BI-RADS assessment obtained an Az improvement from 0.77 to 0.89 (p -value <0.05).

Conclusions

The combination of the proposed CAD system based on SWE features and the BI-RADS assessment would provide a promising diagnostic suggestion.



Keywords

Breast cancer; Shear-wave elastography; Computer-aided diagnosis; Histogram moment; Vector quantification

1. Introduction

Breast lesion characteristics identified with B-mode ultrasound (US) are interpreted to distinguish between benign and malignant lesions in a clinical examination [1]. The description criteria and categories are defined in the **Breast Imaging** Reporting and Data System (BI-RADS) lexicon, which was developed by the American College of **Radiology** [2]. These descriptors, which are quantified in various **computer-aided diagnosis** (CAD) systems [3], [4], [5], [6], [7], [8], [9], [10] to evaluate tumor malignancy, can be classified as morphology and texture characteristics. Recently, elasticity assessment was added as an associated feature of breast US in the fifth edition of **BI-RADS** [2]. Breast cancers such as scirrhous carcinoma and invasive cancers tend to be stiffer than many **benign tumors** [11], [12]. On clinical examination, **elastography** as an **imaging modality** provides additional elasticity information by a cine loop or a single image [13], [14]. Tissue elasticity information can be estimated based on the tissue displacements under a manual or automatic force [15]. According to the elasticity modulus, tissue elasticity is mapped to pixel values in the color elastographic images for display.

Shear-wave elastography (SWE) is an emerging technique that automatically **emits** the radiation force to estimate elasticity with less operator dependence than conventional elastography, which is based on manual compression [15]. Additionally, an observer can evaluate tissue stiffness via only one SWE image rather than a complete image cine loop as in conventional elastography. The SWE image provides tissue elasticity as the velocity of shear waves propagating in tissue and displays the corresponding kilopascals (kPas) on a color map. Using the elasticity information in the map, radiologists can re-evaluate the malignancies of tumors to reduce unnecessary biopsies [16], [17], [18]. However, the qualitative assessment of SWE images through visual observation is user

dependent. To provide an ob

images would be helpful. Ad [Outline](#) [Download](#) [Share](#) [Export](#)

consuming because the number of pixels in a region of interest (ROI) is usually greater than ten thousand (ex: 100×100). In this study, an automated method was proposed to analyze the color patterns in SWE images using individual colors or a combination of color channels. The quantified elasticity information was then used in a CAD system for breast [tumor classification](#). Finally, the performance of a combined CAD system and BI-RADS assessment was evaluated. Using the quantified elasticity features, tumor malignancy could be better evaluated in a more efficient way for clinical use.

2. Materials and methods

2.1. Patients and data acquisition

Our institution review board approved this study, and informed consent was obtained from all patients. From November 2012 to December 2013, 81 patients had undergone [elastography](#) examinations. Three of them had two tumors, and two had three tumors. By [core needle biopsy](#) or [fine-needle aspiration cytology](#), the 88 biopsy-proven cases were classified into 57 benign and 31 malignant tumors. Patients with [benign tumors](#) ranged in age from 26 to 77 years (mean = 50 ± 11). The pathology types were 25 fibrocystic changes, 22 [fibroadenomas](#), and 10 [papillomas](#). The measured sizes were 1.42 ± 1.20 cm. For malignant tumors, patients ranged in age from 30 to 76 years (mean = 54 ± 13). They exhibited 27 [invasive ductal carcinomas](#) (IDC), 1 [invasive lobular carcinoma](#) (ILC), and 3 [ductal carcinoma in situ](#) (DCIS), with measured sizes of 1.51 ± 0.76 cm. Radiologists who were blinded to the pathology report classified the tumors into [BI-RADS](#) assessment categories by B-mode findings. There were 2 (2%) tumors in BI-RADS 2 (benign), 17 (19%) in BI-RADS 3 (probably benign), 52 (59%) in BI-RADS 4 (suspicious abnormality), and 17 (19%) in BI-RADS 5 (highly suggestive of malignancy).

Both B-mode and elastography images were acquired using the Aixplorer ultrasound system (SuperSonic Image, Les Jardins de la Duranne, Aix en Provence, France) with a 5–14 MHz linear broadband transducer (SL15-4). During acquisition, the B-mode image was displayed first to show the anatomical information surrounding the target tumor. A ROI was centered on the target tumor and included tissues around the peritumoral areas to generate an SWE image. The elasticity information is described using Young's modulus, defined as $E = \sigma/\epsilon$ where ϵ is the deformation of the tissue under the applied compression σ . For all cases, the default maximum kPa was 180 (7.7 m/s) in the color display, which is mapped from the value of the elasticity modulus.

2.2. SWE features

The acquired SWE images were color maps that conveyed elasticity information about the tissues. In this study, we proposed extracting a series of quantitative SWE features from the color maps to evaluate tumor elasticity automatically. SWE features included histogram distributions in individual and multiple color channels of the color map. [Spatial correlation](#) was also considered to generate more accurate elasticity features.

2.2.1. Single-channel features

Fig. 1(a) and (b) show shear-w

elasticities of various tissues

[Outline](#)



[Download](#)

[Share](#)

[Export](#)

tumor in Fig. 1(a) are soft and

are shown in colors in the blue range.

By separating the colors in the

image into red (R), green (G), and blue (B) channels, the value distributions of different channels are

distinct. As shown in the histograms in Fig. 1(a), the R and G histograms are left-biased, and the B

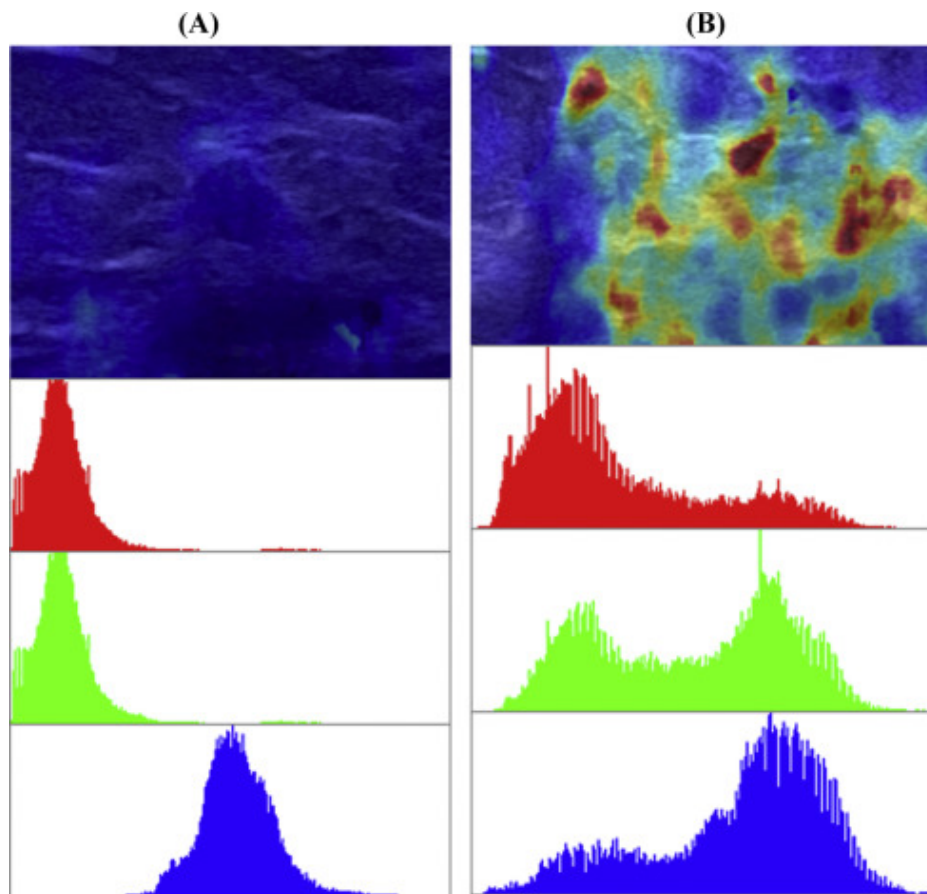
histogram is center-weighted. In contrast, tissues around the malignant tumor in Fig. 1(b) are

shown in various colors, with more well-distributed histograms in the R, G, and B channels.

Consequently, we can compare the differences between histograms to reveal the color composition,

which is the key characteristic to distinguish between benign and malignant tumors in

elastography.



[Download](#) : [Download high-res image \(251KB\)](#)

[Download](#) : [Download full-size image](#)

Fig. 1. Shear-wave elastographic images of two tumors and their corresponding red, green, and blue channels; (a) a benign tumor and (b) a malignant tumor. (For interpretation of the references to color in this figure legend, the reader is referred to the web version of this article.)

By regarding the color distribution in an SWE image as a probability distribution, the color image histogram can be characterized by its moments [19]. Moments [20], [21] are specific quantitative measures of the shape. In the experiment, the 24-bit depth color was decomposed into 8-bit R, G, and B channels. The first-, second-, third-, and fourth-order central moments of the histograms in each channel were calculated to indicate the histogram shape (i.e., mean, variance, skewness, and kurtosis).

$$\text{Mean}_c = \frac{1}{N} \sum_{i=1}^N P_{ci}$$

☰ Outline



Download

Share

Export

$$\text{Variance}_c = \frac{1}{N} \sum_{i=1}^N (P_{ci} - \text{Mean}_c)^2$$

$$\text{Skewness}_c = \frac{1}{N} \sum_{i=1}^N (P_{ci} - \text{Mean}_c)^3 \quad (3)$$

$$\text{Kurtosis}_c = \frac{1}{N} \sum_{i=1}^N (P_{ci} - \text{Mean}_c)^4 \quad (4)$$

where c is the color channel of R, G or B. P_i is the pixel value. Mean is the center location of a distribution calculated by adding up all pixel values and dividing the sum by the number of pixels. Variance is a measure of spread about the mean. Skewness indicates whether the histogram is a symmetric distribution or skewed to one side (left or right side). Kurtosis is a single-peaked histogram with heavy weight in the tails relative to the normal distribution.

A total of 12 single-channel features, including four moments of each of three channels, were calculated: R_{mean} , G_{mean} , B_{mean} , R_{var} , G_{var} , B_{var} , R_{skew} , G_{skew} , B_{skew} , R_{kur} , G_{kur} , and B_{kur} .

2.2.2. Multi-channel features

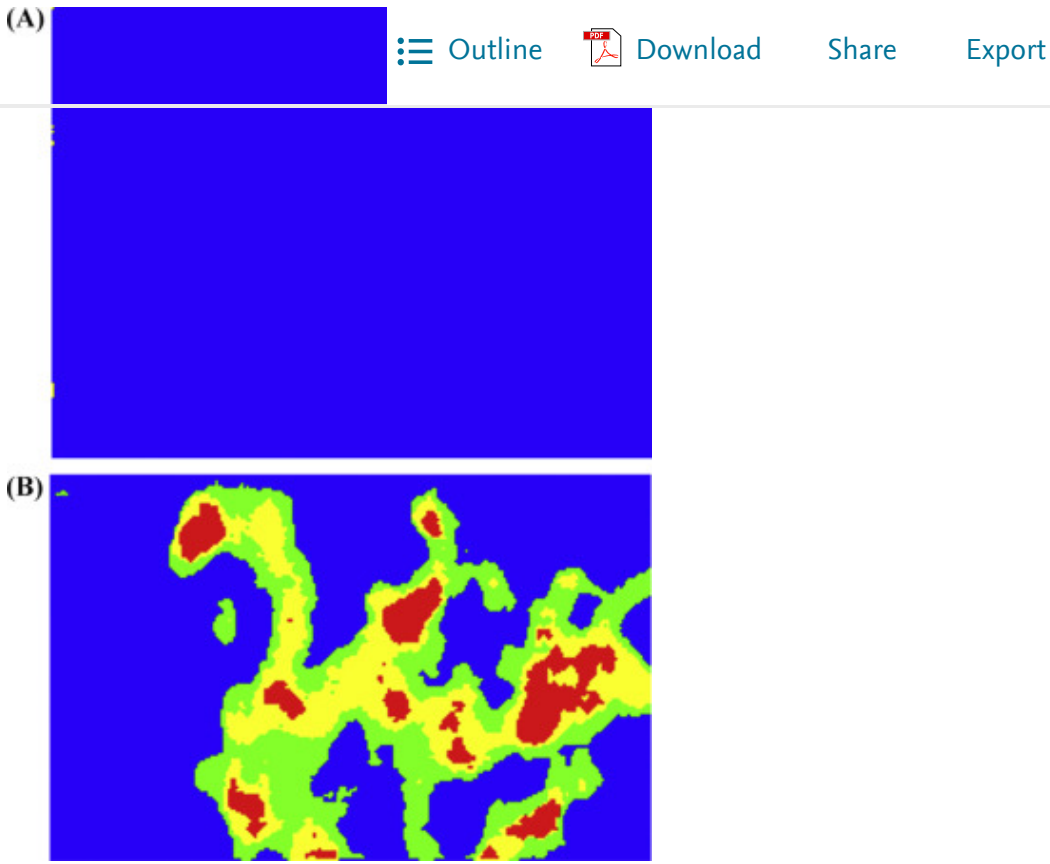
The elasticity levels are shown in different colors in an SWE image. From soft to hard, the colors are continuously encoded from blue to red. The middle color transitions include blue to green, green to yellow, and yellow to red. To emphasize the existence of hard tissues, such as those indicated by yellow and red, [vector quantization](#) [22], [23] was used to reduce the continuous color levels into these four relevant colors for elasticity presentation. The R, G, and B channels of a pixel were joined as a color vector. Based on the vector distances between a color and the four main colors, the image pixels were classified into four clusters. [Euclidean distance](#) was used as the similarity metric in the quantization using the following formula:

$$ED_{PM_i} = \sqrt{(P_R - M_{iR})^2 + (P_G - M_{iG})^2 + (P_B - M_{iB})^2} \quad (5)$$

where ED_{PM_i} is the vector difference between a pixel color P and one of the main colors $M_i = \{\text{blue, green, yellow, red}\}$ in the R, G, and B channels. Each pixel is reassigned a new color according to the nearest color. [Fig. 2](#) shows the quantized color maps of [Fig. 1](#). The numbers of the four-color clusters were divided by the total number of pixels to estimate their ratios in an image: B_{density} , G_{density} , Y_{density} , and R_{density} . A weighted $ColorAvg$ was also calculated by taking the original kPa value into consideration. The definition is:

$$ColorAvg = \frac{B_{Num} \times 36 + G_{Num} \times 72 + Y_{Num} \times 108 + R_{Num} \times 144}{B_{Num} + G_{Num} + Y_{Num} + R_{Num}} \quad (6)$$

where Num is the number of each color after vector quantization.



Download : [Download high-res image \(141KB\)](#)

Download : [Download full-size image](#)

Fig. 2. Quantized color maps comprising four color clusters; (a) quantized Fig. 1(a) and (b) quantized Fig. 1(b).

In addition to the color information, spatial correlation was observed to have an influence on elasticity estimation. In some cases, the areas close to the skin were displayed in stiffness colors relative to the peritumoral areas, as shown in Fig. 3(a). This phenomenon can be regarded as noise because the areas were far from the target tumor. Spatial correlation was thus combined with the kPa-weighted color information to correct for the possible influence automatically. As shown in Fig. 3(b), the spatial weights from the ROI middle to the border are defined as an intensity decreasing function. This feature is defined as following:

$$\mathit{SpatialAvg} = \frac{\sum_P P_{ij}(kPa) \times ((HMid + WMid) - (||P_i - WMid|| + ||P_j - HMid||))}{\sum_P ((HMid + WMid) - (||P_i - WMid|| + ||P_j - HMid||))} \quad (7)$$

where $P_{ij}(kPa)$ is the kPa value of a pixel with i and j as the coordinates; $HMid$ and $WMid$ are the half values of the ROI height and width, respectively; P_i is the coordinate value of a pixel in horizontal; and P_j is the coordinate value of a pixel in vertical.

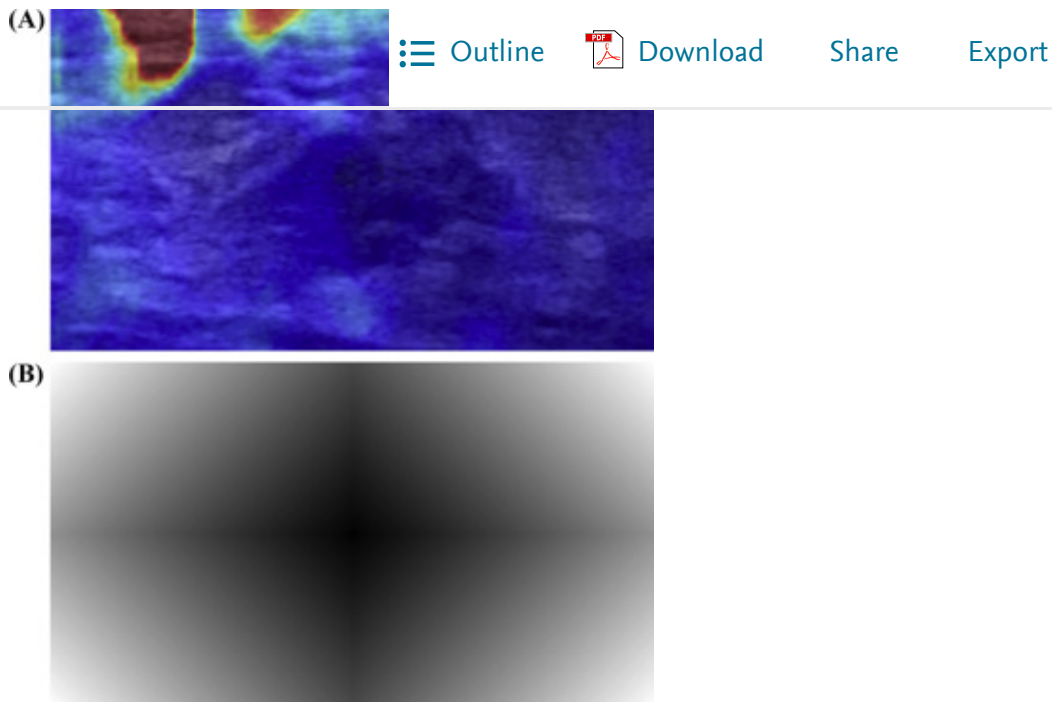


Fig. 3. An illustration of how to combine color and spatial information; (a) the artifact in the skin area is displayed in stiffness colors and (b) the spatial weights from the ROI middle to the border are defined as an intensity decreasing function.

2.3. Performance evaluation

The proposed SWE features were evaluated to determine whether they were statistically significant in distinguishing between benign and malignant tumors. The [Kolmogorov–Smirnov test \[24\]](#) was first used to determine if the value distribution of a feature was normal. Normal-distributed features were tested by Student's *t*-test [24], and non-normal features were tested by the Mann–Whitney *U* test [24]. A *p*-value of less than 0.05 indicates statistical significance.

[Tumor classification](#) was based on the combination of the SWE features. Based on the biopsy-proven pathology, relevant subsets of features were selected in a binary [logistic regression](#) model [25]. During [backward elimination](#), features with the lowest error rate were picked in the trained classifier. For the [generalization ability](#), the leave-one-out cross-validation method [26] was used for evaluation. Each time, one case was left out of all N cases and used to test the trained result with the remaining $N - 1$ cases.

Using the logistic regression formula with the selected features, the probability of the malignancy being a cancer was generated. Different probability thresholds may result in different combinations of sensitivity and specificity. A_z , the area under the receiver operating characteristic (ROC) curve, was used to show the overall trade-offs between sensitivity and specificity. Performance differences were compared by [chi-square test](#) in SPSS software (version 16 for Windows; SPSS, Chicago, IL, USA).

In addition to classifying all

RADS assessment was also ex [Outline](#) [Download](#) [Share](#) [Export](#)

one of many tumor characteristics, elastography features should be combined with B-mode features to obtain more reliable diagnostic results from clinical examinations. The commonly used BI-RADS assessment categories are BI-RADS 3 (probably benign, $\leq 2\%$), BI-RADS 4 (suspicious abnormality, $< 95\%$), and BI-RADS 5 (highly suggestive of malignancy). In other words, the malignancies of tumors in the BI-RADS categories under 5 may need further evaluation with more findings. Therefore, the proposed CAD system was combined with the BI-RADS assessment in the experiment to show the complementary advantages.

3. Results

The differential ability of each SWE feature to distinguish between benign and malignant lesions was tested and is shown in [Table 1](#). p -value < 0.05 is the threshold to determine whether the result is statistically significant. These features were combined in a binary [logistic regression](#) model for diagnosis. A tumor with a predicted probability > 0.5 was regarded as malignant in the results. The diagnostic performance in different [BI-RADS](#) assessment categories was evaluated, as shown in [Table 2](#). In the classification, the CAD system performed poorly in classifying BI-RADS 5 cases but achieved accuracies of 100%, 94%, and 83% for BI-RADS 2, 3, and 4 cases, respectively. Because the BI-RADS 5 cases were highly suggested to be malignant, the CAD system was combined with the BI-RADS assessment by classifying the BI-RADS 5 cases as malignancies. As shown in [Table 3](#), the performance of the CAD system improved, with accuracy rising from 81% to 88% ($A_z = 0.77$ vs. 0.89 , p -value < 0.05). The A_z difference can be observed in [Fig. 4](#).

Table 1. The mean, standard deviation (SD), median, and p -value (Student's t -test or Mann–Whitney U -test) of SWE features in ROIs.

Features	Benign		Malignant		p -value
	Mean \pm SD	Median	Mean \pm SD	Median	
<i>Rmean</i>	0.15 \pm 0.03		0.16 \pm 0.07		0.68
<i>Gmean</i>	0.20 \pm 0.06		0.25 \pm 0.10		0.02*
<i>Bmean</i>	0.58 \pm 0.06		0.56 \pm 0.07		0.15
<i>Rvar</i>		0.009		0.010	0.03*
<i>Gvar</i>	0.02 \pm 0.01		0.03 \pm 0.01		< 0.001 *
<i>Bvar</i>		0.01		0.02	0.03*
<i>Rskew</i>	1.65 \pm 0.96		1.98 \pm 1.06		0.13
<i>Gskew</i>	1.30 \pm 0.71		1.02 \pm 0.69		0.07
<i>Bskew</i>	-0.01 \pm 0.48		-0.46 \pm 0.61		< 0.001 *
<i>Rkur</i>		7.09		10.05	0.38



Mean :

Features	Mean	Std. Dev.	Mean	p-value
<i>Gkur</i>	4.40	0.99	3.82	0.03*
<i>Bkur</i>	3.10	0.99	3.68	0.35
<i>Bdensity</i>	0.99	0.0008	0.94	<0.001*
<i>Gdensity</i>	0.0008	0.0003	0.0320	<0.001*
<i>Ydensity</i>	0.0003	0.000	0.0061	<0.001*
<i>Rdensity</i>	0.000	36.11	0.004	<0.001*
<i>ColorAvg</i>	36.11	36.06	38.91	<0.001*
<i>SpatialAvg</i>	36.06		38.77	<0.001*

*

p-value <0.05 indicates a statistically significant difference.

Table 2. The performance of the proposed CAD system on different **BI-RADS** category cases.

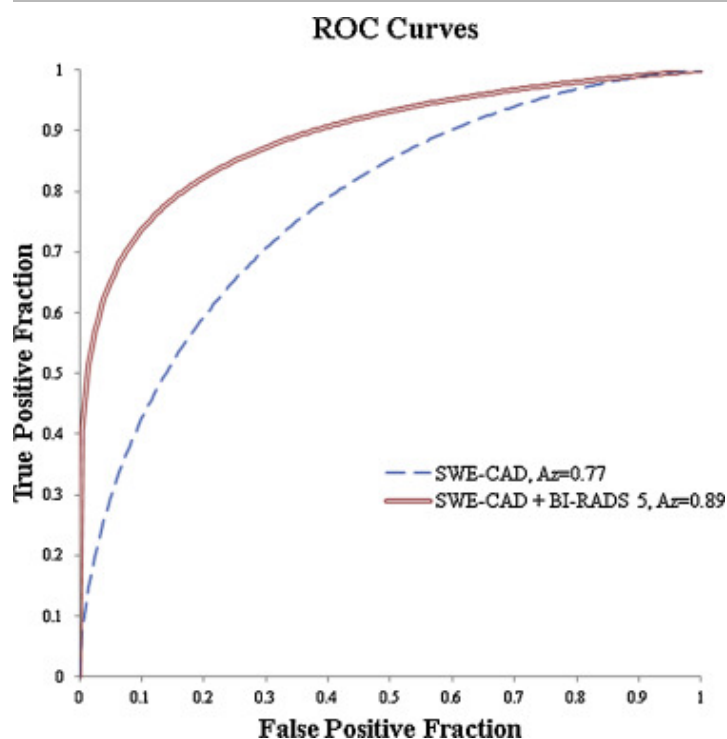
Case category	Accuracy	Sensitivity	Specificity	PPV	NPV
BI-RADS 2	100% (2/2)	N/A	100% (2/2)	N/A	100% (2/2)
BI-RADS 3	94% (16/17)	100% (2/2)	93% (14/15)	67% (2/3)	100% (14/14)
BI-RADS 4	83% (43/52)	54% (7/13)	92% (36/39)	70% (7/10)	86% (36/42)
BI-RADS 5	59% (10/17)	63% (10/16)	0% (0/1)	91% (10/11)	0% (0/6)

Table 3. The performances of different combinations of **BI-RADS** category cases and classifiers.

Classifier	Accuracy	Sensitivity	Specificity	PPV	NPV	Az
Radiologist (BI-RADS 5)	94% (16/17)	100% (16/16)	0% (0/1)	94% (16/17)	N/A	N/A
CAD (BI-RADS 2,3,4,5)	81% (71/88)	61% (19/31)	91% (52/57)	79% (19/24)	81% (52/64)	0.77
CAD (BI-RADS 2,3,4) + Radiologist (BI-RADS 5)	88% (77/88)	81% (25/31)	91% (52/57)	83% (25/30)	90% (52/58)	0.89

*

p-value <0.05 indicates a statistically significant difference.



[Download : Download high-res image \(184KB\)](#)

[Download : Download full-size image](#)

Fig. 4. The ROC curves of the CAD system based on SWE features and the CAD system combined with the BI-RADS assessment.

4. Discussion

The American College of Radiology suggests elasticity assessment as a tool to evaluate breast tumor malignancy in the fifth edition of BI-RADS, released in 2013 [2]. The suggestion indicates that elastography provides additional diagnostic information over conventional B-mode imaging. On clinical examination, a newly developed SWE emits the radiation force to obtain more reproducible results than conventional manual compression. Based on SWE, we extracted various quantitative features in this study to provide a more objective and efficient elasticity evaluation. Twelve features were tested for statistical significance in distinguishing between benign and malignant breast lesions (Table 1). In particular, *SpatialAvg*, which combined spatial and color information, was better than using color information alone (*ColorAvg*). The use of *SpatialAvg* would be helpful in reducing the effect of artifacts in the ROI border. Fig. 1 is a simple example showing that extracting features from the R, G, and B channels to distinguish between benign and malignant tumors is practical. In the experiment, using the mean and standard deviation of the pixel values from the R, G, and B

channels resulted in an accuracy

SWE features (81%). Therefore, [Outline](#) [Download](#) [Share](#) [Export](#)

In addition to the original RGB color space, HSV was also applied in the experiment to provide performance comparisons with different color spaces [27]. The Az achieved by HSV was 0.70, which was lower than the 0.77 achieved by RGB. Combining both color spaces simultaneously resulted in no better performance ($Az = 0.77$). The corresponding ROC curves are illustrated in Fig. 5. HSV is useful in distinguishing between different colors in natural images. However, in the color elastographic images, pixels having similar saturation and brightness values are only different in hue. Therefore, the analysis of RGB may already provide sufficient information. Additionally, using the original RGB values without further color space transformation is efficient.

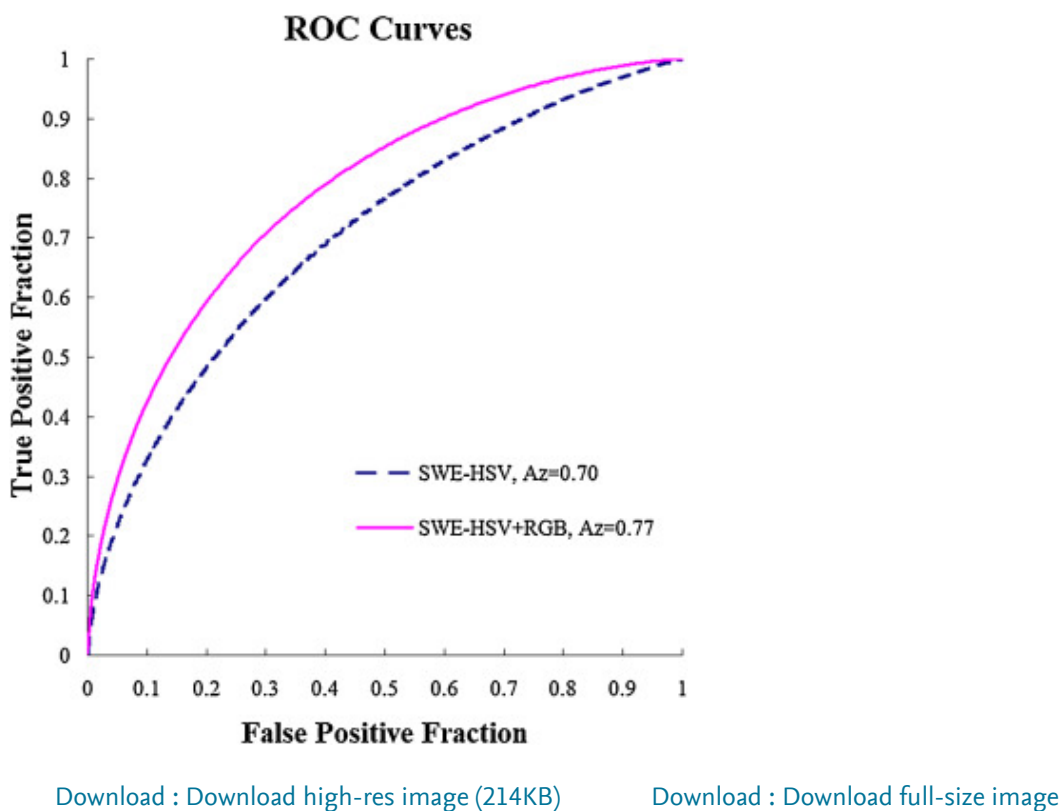


Fig. 5. The ROC curves of the CAD systems based on SWE features extracted from HSV and RGB color spaces.

The performance of the CAD system based on the proposed SWE features achieved an accuracy of 81% with a sensitivity of 61% and a specificity of 91%. The high specificity shows that the elasticity information may be helpful in avoiding unnecessary biopsies. To evaluate the clinical use of the CAD system, the performances of the CAD system on different BI-RADS assessment categories are listed in Table 2. Although tissue elasticity is useful in diagnosis, it is only one of numerous characteristics of malignant tumors. BI-RADS 5 tumors have B-mode findings such as taller-than-wide, irregular shape, spiculation, and hypoechogenicity [1], which could not definitely indicate hard tissues in the tumor area. Therefore, the assessments from elastography and B-mode imaging may not be consistent in the same cases. However, BI-RADS 5 cases are regarded as highly suggestive of malignancy. It is reasonable to keep the B-mode results for BI-RADS 5 cases and

combine the classification re-

sensitivity improved from 61  [Outline](#)  [Download](#) [Share](#) [Export](#)

value = 0.0048). The results are consistent with the studies [19], [27], [28], [29] conducted by human observation showing that tumor elasticity provides additional diagnostic information over B-mode imaging.

The only manual step to generate the proposed SWE features is defining an ROI, which is also a necessary step to generate the elasticity color map in the Aixplorer ultrasound system. Previous CAD systems using SWE features [30] achieved $A_z = 0.97$, which is higher than $A_z = 0.77$ in this study. The combinations of BI-RADS assessments achieved $A_z = 0.973$ and $A_z = 0.89$, respectively. The performance difference may depend on the types of lesions in individual databases. For the image database used in this study, the result suggested to use SWE features for BI-RADS cases with uncertain malignancy to improve the A_z from 0.77 to 0.89 (p -value < 0.05). The advantages of the proposed method are convenience and efficiency. Users may want to use the proposed method if they do not have sophisticated skills for determining whether the segmented contour is good or bad. This method also provides another tool for users who are unsatisfied with the [segmentation](#) results in previous studies [30] because they already have their preferences for contour description. Using user-defined ROI to specify tumor area is a necessary step to generate an SWE image. Consequently, we believe that the proposed method based on ROIs is appropriate for all types of users and has the least operator dependence.

A limitation of this study is how to appropriately select the tumor ROI. To the best of our knowledge, there is no published paper indicating the best way to define the ROI. Prior studies only suggested including peritumoral areas in addition to the tumor itself [31] or using an adaptive ROI size for different tumors [18]. In this experiment, we compared the performances of SWE features extracted from the whole ROI (81%) and the ROI center (72%), which was one-fourth the size of the whole ROI. The results showed that defining the ROI by extending the half size of the tumor from the tumor boundary provides more diagnostic information than using only the tumor itself, which may not provide sufficiently robust results. In future experiments exploring this issue, we will perform tumor segmentation to delineate the tumor contour and explore the effects of different sizes of ROIs derived from the tumor contour for a more complete evaluation.

A possible improvement of the CAD system could be quality inspection. As mentioned previously, artifacts may be induced by overcompression on the probe. An artifact is shown as stiffness color in the skin area, i.e., the boundary of a ROI. CAD can detect an artifact automatically and trigger a quality alarm or ignore the inaccurate information. Another future study will integrate the quantitative features in B-mode imaging into the CAD system. A totally automated diagnostic procedure, including the information from SWE and B-mode images, would be an efficient tool in clinical use.

5. Conclusions

A CAD system based on the quantitative SWE features was developed in this study to distinguish malignant from benign breast tumors. Combining the CAD system with a [BI-RADS](#) assessment achieved an improved $A_z = 0.89$ (p -value < 0.05) which would provide promising diagnostics in clinical use.

Conflict of interest

The authors declare that they  [Outline](#)  [Download](#) [Share](#) [Export](#)

organizations that could inappropriately influence their work.

Acknowledgments

The authors thank the Ministry of Science and Technology (MOST 103-2221-E-002-170-MY3) and Ministry of Education (AE-00-00-06) of the Republic of China for the financial support.

[Recommended articles](#)

[Citing articles \(21\)](#)

References

- [1] A.T. Stavros, D. Thickett, C.L. Rapp, M.A. Dennis, S.H. Parker, G.A. Sisney
Solid breast nodules: use of sonography to distinguish between benign and malignant lesions
Radiology, 196 (1995), pp. 123-134
[CrossRef](#) [View Record in Scopus](#) [Google Scholar](#)
- [2] American College of Radiology
Breast Imaging Reporting and Data System: ACR BI-RADS—Breast Imaging Atlas
(5th ed.), American College of Radiology, Reston, VA (2013)
[Google Scholar](#)
- [3] T. Sun, J. Wang, X. Li, P. Lv, F. Liu, Y. Luo, Q. Gao, H. Zhu, X. Guo
Comparative evaluation of support vector machines for computer aided diagnosis of lung cancer in CT based on a multi-dimensional data set
Comput. Methods Progr. Biomed., 111 (2013), pp. 519-524
[Article](#)  [Download PDF](#) [View Record in Scopus](#) [Google Scholar](#)
- [4] H. Mohamed, M.S. Mabrouk, A. Sharawy
Computer aided detection system for micro calcifications in digital mammograms
Comput. Methods Progr. Biomed., 116 (2014), pp. 226-235
[Article](#)  [Download PDF](#) [View Record in Scopus](#) [Google Scholar](#)
- [5] W.K. Moon, C.-M. Lo, J.M. Chang, C.-S. Huang, J.-H. Chen, R.-F. Chang
Computer-aided classification of breast masses using speckle features of automated breast ultrasound images
Med. Phys., 39 (2012), pp. 6465-6473
[CrossRef](#) [View Record in Scopus](#) [Google Scholar](#)
- [6] W.K. Moon, C.-M. Lo, N. Cho, J.M. Chang, C.-S. Huang, J.-H. Chen, R.-F. Chang
Computer-aided diagnosis of breast masses using quantified BI-RADS findings
Comput. Methods Progr. Biomed., 111 (2013), pp. 84-92
[Article](#)  [Download PDF](#) [View Record in Scopus](#) [Google Scholar](#)
- [7] Y.-H. Huang, Y.-C. Chang, C.-S. Huang, T.-J. Wu, J.-H. Chen, R.-F. Chang

- [8] K.G. Kim, S.W. Cho, S.J. Min, J.H. Kim, B.G. Min, K.T. Bae
Computerized scheme for assessing ultrasonographic features of breast masses
Acad. Radiol., 12 (2005), pp. 58-66
[Article](#)  [Download PDF](#) [View Record in Scopus](#) [Google Scholar](#)
- [9] C.-M. Lo, R.-T. Chen, Y.-C. Chang, Y.-W. Yang, M.-J. Hung, C.-S. Huang, R.-F. Chang
Multi-dimensional tumor detection in automated whole breast ultrasound using topographic watershed
IEEE Trans. Med. Imaging, 33 (2014), pp. 1503-1511
[CrossRef](#) [View Record in Scopus](#) [Google Scholar](#)
- [10] K. Drukker, M.L. Giger, C.E. Metz
Robustness of computerized lesion detection and classification scheme across different breast US platforms 1
Radiology, 237 (2005), pp. 834-840
[CrossRef](#) [View Record in Scopus](#) [Google Scholar](#)
- [11] E. Fleury, J. Fleury, S. Piato, D. Roveda Jr.
New elastographic classification of breast lesions during and after compression
Diagn. Interv. Radiol., 15 (2009), pp. 96-103
[Google Scholar](#)
- [12] C.W. Sewell
Pathology of benign and malignant breast disorders
Radiol. Clin. N. Am., 33 (1995), pp. 1067-1080
[View Record in Scopus](#) [Google Scholar](#)
- [13] N. Cho, W.K. Moon, J.M. Chang, A. Yi, H.R. Koo, J.-S. Park, I.A. Park
Sonoelastographic lesion stiffness: preoperative predictor of the presence of an invasive focus in nonpalpable DCIS diagnosed at US-guided needle biopsy
Eur. Radiol., 21 (2011), pp. 1618-1627
[CrossRef](#) [View Record in Scopus](#) [Google Scholar](#)
- [14] C.M. Lo, Y.P. Chen, Y.C. Chang, C. Lo, C.S. Huang, R.F. Chang
Computer-aided strain evaluation for acoustic radiation force impulse imaging of breast masses
Ultrason. Imaging, 36 (2014), p. 151
[CrossRef](#) [View Record in Scopus](#) [Google Scholar](#)
- [15] K. Nightingale
Acoustic radiation force impulse (ARFI) imaging: a review
Curr. Med. Imaging Rev., 7 (2011), p. 328
[CrossRef](#) [View Record in Scopus](#) [Google Scholar](#)

Breast lesions: quantitative elastography with superresolution imaging preliminary results 1

Radiology, 256 (2010), pp. 297-303

[CrossRef](#) [View Record in Scopus](#) [Google Scholar](#)

- [17] W.A. Berg, D.O. Cosgrove, C.J. Doré, F.K. Schäfer, W.E. Svensson, R.J. Hooley, R. Ohlinger, E.B. Mendelson, C. Balu-Maestro, M. Locatelli
Shear-wave elastography improves the specificity of breast US: the BE1 multinational study of 939 masses

Radiology, 262 (2012), pp. 435-449

[CrossRef](#) [View Record in Scopus](#) [Google Scholar](#)

- [18] A. Evans, P. Whelehan, K. Thomson, D. McLean, K. Brauer, C. Purdie, L. Jordan, L. Baker, A. Thompson

Quantitative shear wave ultrasound elastography: initial experience in solid breast masses

Breast Cancer Res., 12 (2010), p. R104

[Google Scholar](#)

- [19] H.J. Baek, H.S. Kim, N. Kim, Y.J. Choi, Y.J. Kim
Percent change of perfusion skewness and kurtosis: a potential imaging biomarker for early treatment response in patients with newly diagnosed glioblastomas

Radiology, 264 (2012), pp. 834-843

[CrossRef](#) [View Record in Scopus](#) [Google Scholar](#)

- [20] D. Đorić, E. Nikolić-Đorić, V. Jevremović, J. Mališić
On measuring skewness and kurtosis

Qual. Quant., 43 (2009), pp. 481-493

[CrossRef](#) [View Record in Scopus](#) [Google Scholar](#)

- [21] R.A. Groeneveld, G. Meeden
Measuring skewness and kurtosis

Statistician (1984), pp. 391-399

[CrossRef](#) [View Record in Scopus](#) [Google Scholar](#)

- [22] M.T. Orchard, C.A. Bouman
Color quantization of images

IEEE Trans. Signal Process., 39 (1991), pp. 2677-2690

[CrossRef](#) [View Record in Scopus](#) [Google Scholar](#)


- [23] P.-C. Huang, P.-C. Li
Vector quantization of RF channel data for ultrasound imaging

Ultrason. Imaging, 35 (2013), pp. 3-16

[CrossRef](#) [View Record in Scopus](#) [Google Scholar](#)

- [24] A.P. Field
Discovering Statistics Using SPSS



- [25] D.W. Hosmer
Applied Logistic Regression
(2nd ed.), Wiley, New York (2000)
[Google Scholar](#)
- [26] E. Alpaydin
Introduction to Machine Learning
MIT Press, Cambridge, MA (2004)
[Google Scholar](#)
- [27] Y. Xiao, J. Wu, J. Yuan
mCENTRIST: a multi-channel feature generation mechanism for scene categorization
IEEE Trans. Image Process., 23 (2014), pp. 823-836
[CrossRef](#) [View Record in Scopus](#) [Google Scholar](#)
- [28] A. Evans, P. Whelehan, K. Thomson, K. Brauer, L. Jordan, C. Purdie, D. McLean, L. Baker, S. Vinnicombe, A. Thompson
Differentiating benign from malignant solid breast masses: value of shear wave elastography according to lesion stiffness combined with greyscale ultrasound according to BI-RADS classification
Br. J. Cancer, 107 (2012), pp. 224-229
[CrossRef](#) [View Record in Scopus](#) [Google Scholar](#)
- [29] J.H. Youk, H.M. Gweon, E.J. Son, K.H. Han, J.-A. Kim
Diagnostic value of commercially available shear-wave elastography for breast cancers: integration into BI-RADS classification with subcategories of category 4
Eur. Radiol., 23 (2013), pp. 2695-2704
[CrossRef](#) [View Record in Scopus](#) [Google Scholar](#)
- [30] Y. Xiao, J. Zeng, L. Niu, Q. Zeng, T. Wu, C. Wang, R. Zheng, H. Zheng
Computer-aided diagnosis based on quantitative elastographic features with supersonic shear wave imaging
Ultrasound Med. Biol., 40 (2014), pp. 275-286
[Article](#)  [Download PDF](#) [View Record in Scopus](#) [Google Scholar](#)
- [31] J.M. Chang, W.K. Moon, N. Cho, A. Yi, H.R. Koo, W. Han, D.-Y. Noh, H.-G. Moon, S.J. Kim
Clinical application of shear wave elastography (SWE) in the diagnosis of benign and malignant breast diseases
Breast Cancer Res. Treat., 129 (2011), pp. 89-97
[CrossRef](#) [View Record in Scopus](#) [Google Scholar](#)

[View Abstract](#)

[About ScienceDirect](#)[Remote access](#)[Shopping cart](#)[Advertise](#)[Contact and support](#)[Terms and conditions](#)[Privacy policy](#)

We use cookies to help provide and enhance our service and tailor content and ads. By continuing you agree to the **use of cookies**.

Copyright © 2020 Elsevier B.V. or its licensors or contributors. ScienceDirect® is a registered trademark of Elsevier B.V.

ScienceDirect® is a registered trademark of Elsevier B.V.

